ELSEVIER

Physica D 147 (2000) 12–35

PHYSICA D

www.elsevier.com/locate/physd

Exit-times and ϵ-entropy for dynamical systems, stochastic processes, and turbulence

M. Abel [a,b], L. Biferale [c,d], M. Cencini [e], M. Falcioni [a,b,*], D. Vergni [a,b], A. Vulpiani [a,b]

[a] *Dipartimento di Fisica, Universitá di Roma "La Sapienza", p.le Aldo Moro 2, I-00185 Rome, Italy*
[b] *INFM, p.le Aldo Moro 2, I-00185 Rome, Italy*
[c] *Dipartimento di Fisica, Universitá di Roma "Tor Vergata", via della Ricerca Scientifica 1, 00133 Rome, Italy*
[d] *INFM, via della Ricerca Scientifica 1, 00133 Rome, Italy*
[e] *Max-Planck-Institut für Physik Komplexer Systeme, Nöthnitzer Str. 38, 01187 Dresden, Germany*

Received 22 March 2000; received in revised form 3 July 2000; accepted 3 July 2000
Communicated by U. Frisch

Abstract

We present an investigation of ϵ-entropy, $h(\epsilon)$, in dynamical systems, stochastic processes and turbulence. This tool allows for a suitable characterization of dynamical behaviours arising in systems with many different scales of motion. Particular emphasis is put on a recently proposed approach to the calculation of the ϵ-entropy based on the exit-time statistics. The advantages of this method are demonstrated in examples of deterministic diffusive maps, intermittent maps, stochastic self- and multi-affine signals and experimental turbulent data. Concerning turbulence, the multifractal formalism applied to the exit-time statistics allows us to predict that $h(\epsilon) \sim \epsilon^{-3}$ for velocity–time measurement. This power law is independent of the presence of intermittency and has been confirmed by the experimental data analysis. Moreover, we show that the ϵ-entropy density of a three-dimensional velocity field is affected by the correlations induced by the sweeping of large scales.

PACS: 05.45.−a; 47.27.Eq

Keywords: Entropy; Coding theory; Turbulence; Multifractals

1. Introduction

Many sciences, ranging from geophysics to economics, share the crucial problem of extracting information about the underlying dynamics of a system through the analysis of data time series [1]. In these investigations, a central role is played by the evaluation of the complexity degree of a string of data as a way to probe the underlying dynamics [2,3]. Since the pioneering works of Shannon on information theory [4,5], entropy has been proposed as the proper mathematical tool to quantitatively address such a question. Nowadays, entropy constitutes a key-concept to answer questions ranging from the more conceptual aim to distinguish a pure stochastic evolution from a chaotic

* Corresponding author. Address: Dipartimento di Fisica, Universitá di Roma "La Sapienza", p.le Aldo Moro 2, I-00185 Rome, Italy. Fax: +39-06-4463158
E-mail address: massimo.falcioni@roma1.infn.it (M. Falcioni).

0167-2789/00/$ – see front matter
PII: S0167-2789(00)00147-0

deterministic one to the more applied goal of quantifying the degree of predictability at varying the space–time resolution [6–11]. The latter question is evidently of primary importance, e.g., to set the proper resolution of the data accumulation rate in experimental settings or to efficiently compress data which have to be stored or transmitted.

The distinction between stochastic and deterministic chaotic evolution can be formalized by introducing the Kolmogorov–Sinai (KS) entropy, h_{KS} [12,13]. Let us consider a time series x_t (with $t = 1, \ldots, T$) where, for simplicity, the time is discretized but x_t is a continuous variable. By defining a finite partition of the phase-space, where each element of the partition has diameter smaller than ϵ, and by recording for each t the symbol (letter) identifying the cell x_t belongs to, one can code the time series into a sequence of symbols out of a finite alphabet. Then, from the probabilities of words of length m (m-words) one can compute the m-block entropy. Finally, one measures the information-gain in going from m-words to $(m+1)$-words: in the limit of infinitely long words ($m \to \infty$) and of arbitrary fine partition ($\epsilon \to 0$) one obtains h_{KS}, i.e. an entropy per unit time [6]. Naturally, this limit cannot be carried out for any real data due to the finite sampling time and resolution of any experimental set-up. The value of h_{KS} characterizes the process which has generated the time series. For example, in a continuous stochastic evolution, which reveals more and more unpredictable outcomes at increasing the resolution, the KS-entropy is infinite. On the other hand, a regular deterministic signal is characterized by a zero KS-entropy, since it is completely predictable after a finite number of observations, at any given resolution. Between these two limiting cases, a finite positive value of h_{KS} is the signature of a deterministic chaotic dynamics. The KS-entropy measures the growth rate of unpredictability of the evolution, which coincides with the rate of information acquisition necessary to unambiguously reconstruct the signal. However, the distinction between chaotic and stochastic dynamics can be troublesome in practical application (see [11] for a related discussion). Indeed, only in simple, low-dimensional, dynamical systems the h_{KS} evaluation can be properly carried out. As soon as one has to cope with realistic systems, e.g., geophysical flows, the number of degrees of freedom is so large that it inhibits any definite statement based on the KS-entropy evaluation. Moreover, even if one were able to compute the KS-entropy of those systems, many interesting features cannot be answered by only knowing h_{KS}. As a relevant example we mention the case of turbulence, the dynamics of which is characterized by a hierarchy of fluctuations with different characteristic times and spatial scales [14]. In this respect the KS-entropy is related only to the fastest timescale present in the dynamics. Therefore, to quantify the predictability degree or entropy production, respectively, depending on the analysed range of scales and frequencies, we need a more general tool [8–10,15]. In order to make a step to overcome these difficulties, we consider a scale-dependent quantity, namely the ϵ-entropy, $h(\epsilon)$, originally introduced by Shannon [4,5] and Kolmogorov [16,17] to characterize continuous processes. It is remarkable that, in spite of its deep relevance for the characterization of stochastic processes and non-trivial dynamical systems, the ϵ-entropy is not widely used in the physical community. Only recently, mainly after the review paper of Gaspard and Wang [8] and the introduction of the finite size Lyapunov exponent [9,10], there appeared some attempts in the use of the ϵ-entropy. For this reason, in Section 2 we give a brief pedagogical review, aimed to introduce the reader to the ϵ-entropy and (ϵ, τ)-entropy. Practically the (ϵ, τ)-entropy, $h(\epsilon, \tau)$, is the Shannon-entropy of timeseries sampled at frequency τ^{-1} and measured with an accuracy ϵ in the phase-space. We will see that the analysis of the ϵ-dependence of $h(\epsilon)$ is able to highlight many dynamical features of very high-dimensional systems like turbulence as well as of stochastic processes [8,15]. The determination of $h(\epsilon, \tau)$ is usually performed, as already stated, by looking at the Shannon-entropy of the coarse-grained dynamics on a (ϵ, τ) grid in phase-space. Unfortunately, this method suffers of so many computational drawbacks that it is almost unusable in many interesting situations. In particular, it is very inefficient when one investigates phenomena arising from the complex interplay of many different spatial and temporal scales, the ones we are interested in. Therefore, here we resort to a recently proposed method [18] based on the *exit-time* analysis, which has been demonstrated to be both practically and conceptually advantageous with respect to the standard one. In a few words, the idea consists in looking at a sequence of data not at fixed sampling time but at fixed fluctuation, i.e. when the signal is larger than some given threshold, ϵ. This procedure allows a

noticeable improvement of the computational possibility to measure the ϵ-entropy. We give an ample demonstration of the advantages of this method in a number of examples ranging from one-dimensional dynamical systems, to stochastic (affine and multi-affine) processes and turbulence.

As far as turbulence is concerned, we present both an application to experimental data analysis and a theoretical remark. Namely, we will see that from the computation of the ϵ-entropy of turbulent flows one has a deep understanding of the spatial correlation induced by the sweeping of large scales on the smaller ones. In order to understand these features we also introduce and discuss a new stochastic model of turbulent flows which takes into account sweeping effects.

The ϵ-entropy, allows for a rather general and feasible analysis for the investigation of the dynamical properties of systems characterized by the coexistence of many degrees of freedom and characteristic times. At variance with other (more popular) quantities as Lyapunov exponents and KS-entropy, the ϵ-entropy has a rather wide range of applicability also in experimental data analysis, where arbitrary fine resolution cannot be reached. The exit-times approach to the ϵ-entropy is an efficient method to its computation.

The paper is organized as follows. In Section 2, we briefly define the ϵ-entropy and discuss its properties; we use a simple example which shows the conceptual relevance of this quantity together with the difficulties of its computation. In Section 3, we introduce the *exit-time* approach to the calculation of the ϵ-entropy discussing in detail its theoretical and numerical advantages. In Section 4, we discuss the use of the ϵ-entropy in characterizing intermittent low-dimensional dynamical systems and stochastic (affine and multi-affine) processes. In Section 5, we present a study of high-Reynolds experimental data and a theoretical analysis of the ϵ-entropy in turbulence. Some conclusions and remarks follow in Section 6. Details on the stochastic model of a turbulent field are discussed in Appendices A and B.

2. The ϵ-entropy

Assume a given time-continuous record of one observable, $x(t) \in \mathbb{R}$, over a total time T long enough to ensure a good statistics. For the sake of simplicity, we start considering x as an observable of a one-dimensional system.

The estimate of the entropy of the time record $x(t)$ requires the construction of a symbolic dynamics [4–6,8]. With this purpose, one considers, as a first step, a grid on the time axis, by introducing a small time interval, τ, so as to obtain a sequence $\{x_i = x(t_i), i = 1, \ldots, N\}$ with $N = [T/\tau]$ ($[\cdot]$ denotes the integer part). As a second operation, one performs a coarse-graining of the phase-space, with a grid of mesh size ϵ, and defines a set of symbols, $\{S\}$ (the letters of the alphabet), that biunivocally correspond to the so-formed cells. Then, one has to consider the different words of length n, out of the complete sequence of symbols:

$$W_k^n(\epsilon, \tau) = (S_k, S_{k+1}, \ldots, S_{k+n-1}),$$

where S_j labels the cell containing x_j. See Fig. 1, where the above codification is sketched. From the probability distribution $P(W^n(\epsilon, \tau))$, estimated from the words frequencies, one calculates the block entropies $H_n(\epsilon, \tau)$:

$$H_n(\epsilon, \tau) = -\sum_{\{W^n(\epsilon,\tau)\}} P(W^n(\epsilon, \tau)) \ln P(W^n(\epsilon, \tau)), \tag{1}$$

where $\{W^n(\epsilon, \tau)\}$ indicates the set of all possible words of length n. The (ϵ, τ)-entropy per unit time, $h(\epsilon, \tau)$, is finally defined as

$$h_n(\epsilon, \tau) = \frac{1}{\tau}[H_{n+1}(\epsilon, \tau) - H_n(\epsilon, \tau)], \tag{2}$$

$$h(\epsilon, \tau) = \lim_{n\to\infty} h_n(\epsilon, \tau) = \frac{1}{\tau} \lim_{n\to\infty} \frac{1}{n} H_n(\epsilon, \tau). \tag{3}$$

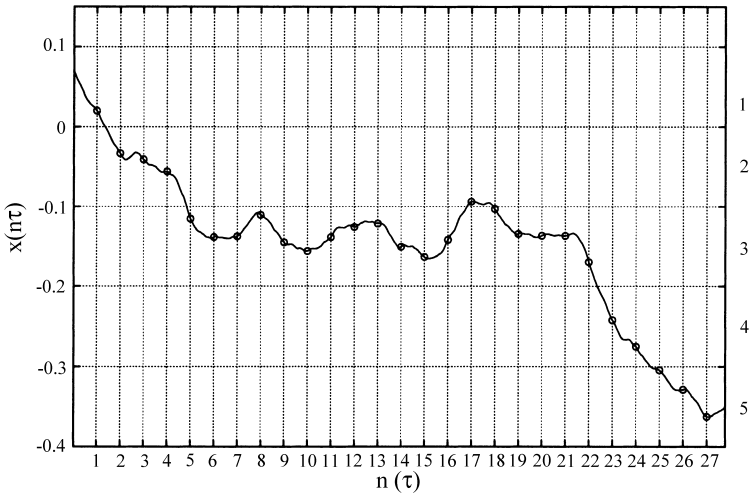

Fig. 1. Sketch of the coding procedure described in Section 2. On the given (ϵ, τ)-grid the symbolic sequence is $W_0^{27}(\epsilon, \tau) = (1, 2, 2, 2, 3, 3, 3, 3, 3, 3, 3, 3, 3, 3, 3, 3, 2, 3, 3, 3, 3, 3, 4, 4, 5, 5, 5)$.

For practical reasons the dependence on the details of the partition is ignored, while the rigorous definition is given in terms of the infimum over all possible partitions with elements of diameter smaller than ϵ [6,8]. As far as we know, it is possible to carry out the computation of the ϵ-entropy according to the rigorous mathematical definition only in few peculiar systems, e.g., in stationary Gaussian processes [16,17]. Therefore, in practice, one is forced to choose a certain feasible ϵ-partition, as, e.g., the previously described one. The above defined (ϵ, τ)-entropy is nothing but the Shannon-entropy of the sequence of symbols $\{S_i\}$. In the case of the time-continuous evolutions, whose realizations are continuous functions of time, the τ dependence of $h(\epsilon, \tau)$ does not exist [6,19]. When this happens, one has a finite ϵ-entropy per unit time, $h(\epsilon)$. For genuine time-discrete systems, one can simply put $h(\epsilon) \equiv h(\epsilon, \tau = 1)$. In all these cases,

$$h_{\mathrm{KS}} = \lim_{\epsilon \to 0} h(\epsilon). \tag{4}$$

The determination of h_{KS} involves the study of the limits $n \to \infty$ and $\epsilon \to 0$ which are in principle independent, but in all practical cases one has to find an optimal choice of the parameters such that the estimated entropy is close to the exact value [1,11].

For a genuine chaotic system, one has $0 < h_{\mathrm{KS}} < \infty$, i.e. the rate of information creation is finite. On the other hand, for a continuous random process, $h_{\mathrm{KS}} = \infty$. Therefore, in order to distinguish between a purely deterministic system and a stochastic system it is necessary to perform the limit $\epsilon \to 0$. Unfortunately, from a physical or numerical point of view this is extremely difficult. Nevertheless, by looking at the behaviour of the ϵ-entropy of the signal at varying ϵ one can have some qualitative and quantitative insights on the chaotic or stochastic nature of the underlying process [11]. Moreover, for some stochastic processes one can explicitly give an estimate of the entropy scaling behaviour of ϵ-entropy [8]. For instance, in the case of a stationary Gaussian process with spectrum $S(\omega) \propto \omega^{-2}$, Kolmogorov [16,17] has rigorously derived

$$h(\epsilon) \sim \frac{1}{\epsilon^2} \tag{5}$$

for small ϵ. However, as we show in the following simple but non-trivial example there are many practical difficulties

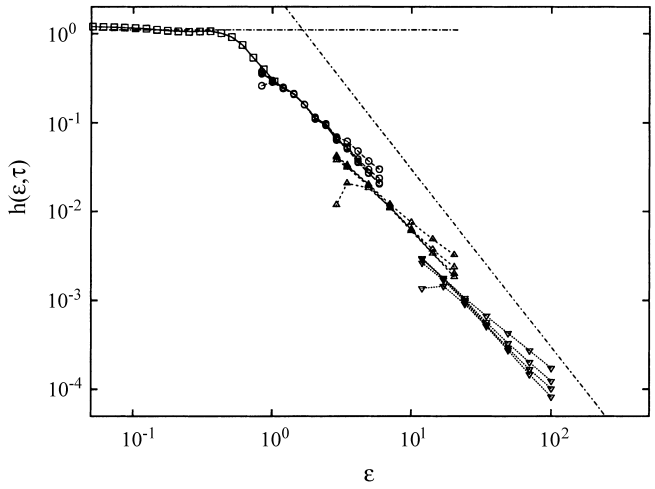

Fig. 2. Numerically evaluated (ϵ, τ)-entropy for the map (6) with $p = 0.8$ computed with the Grassberger–Procaccia algorithm [7] at $\tau = 1$ ($\circ$), $\tau = 10$ ($\triangle$) and $\tau = 100$ ($\triangledown$) and different block lengths ($n = 4, 8, 12, 20$). The boxes ($\square$) give the entropy computed with $\tau = 1$ by using periodic boundary condition over 40 cells. The latter is necessary in order to compute the Lyapunov exponent $\lambda = h_{\mathrm{KS}} = 1.15$. The straight lines correspond to the two asymptotic behaviours, $h(\epsilon) = h_{\mathrm{KS}}$ and $h(\epsilon) \sim \epsilon^{-2}$.

in the computation of $h(\epsilon)$ [11,18]. Let us consider the chaotic map

$$x_{t+1} = x_t + p \sin 2\pi x_t, \tag{6}$$

which for $p > 0.7326\ldots$ produces large scale diffusive behaviour [20], i.e.

$$\langle (x_t - x_0)^2 \rangle \simeq 2Dt \quad \text{for } t \to \infty, \tag{7}$$

where D is the diffusion coefficient. By computing the ϵ-entropy of this system one expects [8,18]

$$h(\epsilon) \simeq \lambda \quad \text{for} \epsilon \lesssim 1, \qquad h(\epsilon) \propto \frac{D}{\epsilon^2} \quad \text{for} \epsilon \gtrsim 1, \tag{8}$$

where λ is the Lyapunov exponent. In Fig. 2 we show that the numerical computation of $h(\epsilon)$, using the standard codification (Fig. 1) is highly non-trivial already in this simple system. Indeed the behaviour (8) in the diffusive region is just poorly obtained by considering the envelope of $h_n(\epsilon, \tau)$ computed for different values of τ; while looking at any single (small) value of τ (one would like to put $\tau = 1$) one obtains a rather inconclusive result. This is due to the fact that one has to consider very large block lengths, n, in order to obtain a good convergence for $H_{n+1}(\epsilon, \tau) - H_n(\epsilon, \tau)$ in (3). In the diffusive regime, a dimensional argument shows that the characteristic time of the system at scale ϵ is $T_\epsilon \approx \epsilon^2/D$. If we consider, e.g., $\epsilon = 10$ and typical values of the diffusion coefficient $D \simeq 10^{-1}$, the characteristic time, T_ϵ, is much larger than the elementary sampling time $\tau = 1$.

Concluding this section, we remind that for systems living in $d > 1$ dimensions, the procedure sketched above, for the determination of $h(\epsilon, \tau)$, goes unaltered, considering that the set of symbols $\{S\}$ now identifies cells in the d-dimensional space where the state-vector $\mathbf{x}(t)$ evolves.

3. How to compute the ϵ-entropy with exit-times

The approach we propose to calculate $h(\epsilon)$ differs from the usual one in the procedure to construct the coding sequence of the signal at a given level of accuracy [18]. This is an important point because the quality of the coding

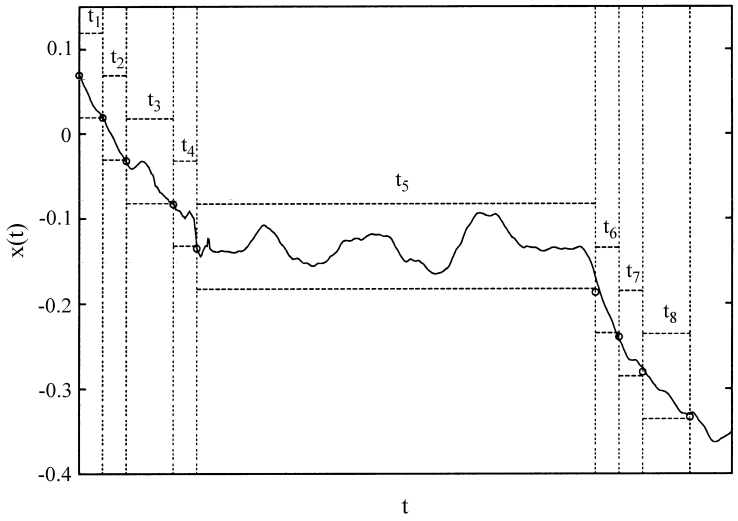

Fig. 3. The same signal as in Fig. 1, with the exit-time coding of the same precision ϵ. The symbolic sequence obtained with the exit-time method is $\Omega_0^{27} = [(t_1, -1); (t_2, -1); (t_3, -1); (t_4, -1); (t_5, -1); (t_6, -1); (t_7, -1); (t_8, -1)]$.

affects largely the result of the ϵ-entropy computation. An efficient procedure reduces redundancy and improves the quality of the results. The problem to encode signals efficiently is quite old and widely discussed in the literature [3,21]. The most efficient compression or codification of a symbolic sequence is linked to its Shannon-entropy. The Shannon's compression theorem [4,5] states: given an alphabet with m symbols, and a sequence of these symbols, $\{S_i, i = 1, \ldots, N\}$ with entropy h, it is not possible to construct another sequence $\{S'_i, i = 1, \ldots, N'\}$ — using the same alphabet and containing the same information — whose length N' is smaller than $(h/\ln m)N$. That is to say: $h/\ln m$ is the maximum allowed compression rate. As a consequence, if one is able to map a sequence $\{s_i, i = 1, \ldots, N_s\}$ of m symbols, into another sequence $\{\sigma_i, i = 1, \ldots, N_\sigma\}$, with the same symbols, the ratio $(N_\sigma/N_s)\ln m$ gives an upper bound for the entropy of $\{s_i\}$. More generally, if $\{\sigma_i\}$ is a codification of $\{s_i\}$ without information loss, then the two sequences must have equal total entropy: $N_s h(s) = N_\sigma h(\sigma)$.

Now we introduce the coding of the signal by the exit-time, $t(\epsilon)$, i.e. the time for the signal to undergo a fluctuation of size ϵ. To do so, we define an alternating grid of cell size ϵ in the following way: we consider the original continuous-time record $x(t)$ and a reference starting time $t = t_0$. The first exit-time, t_1, is then defined as the first time necessary to have an absolute variation equal to $\frac{1}{2}\epsilon$ in $x(t)$, i.e. $|x(t_0 + t_1) - x(t_0)| \geq \frac{1}{2}\epsilon$. This is the time the signal takes to exit the actual cell of size ϵ. Then we restart from t_1 to look for the next exit-time t_2, i.e. the first time such that $|x(t_0 + t_1 + t_2) - x(t_0 + t_1)| \geq \frac{1}{2}\epsilon$ and so on, to obtain a sequence of exit-times: $\{t_i(\epsilon)\}$. To distinguish the direction of the exit (up or down out of a cell), we introduce the label $k_i = \pm 1$, depending on whether the signal is exiting above or below. For clarifying the procedure see Fig. 3, where we sketch the coding method for the signal shown in Fig. 1.

From Fig. 3 one recognizes the alternating structure of the grid: the starting point to find t_{i+1} lies in the middle of the cell $x(t_i) \pm \frac{1}{2}\epsilon$, whereas it lies on the border of the cell $x(t_{i-1}) \pm \frac{1}{2}\epsilon$. In this way one avoids the fast exit of a cell due to small fluctuations (compare Figs. 1 and 3). At the end of this construction, the trajectory is coded without ambiguity, with the required accuracy, by the sequence $\{(t_i, k_i), i = 1, \ldots, M\}$, where M is the total number of exit-time events observed during the total time T. A continuous signal, evolving in a continuous time, is now coded in two sequences — a discrete-valued one $\{k_i\}$ and a continuous-valued one $\{t_i\}$. Performing a coarse-graining of the possible values assumed by $t(\epsilon)$ by the resolution time τ_r, we accomplished the goal of obtaining a symbolic

sequence. After that, one proceeds as usual, studying the "exit-time words" of various lengths n. These are the subsequences of couples of symbols

$$\Omega_i^n(\epsilon, \tau_r) = ((\eta_i, k_i), (\eta_{i+1}, k_{i+1}), \ldots, (\eta_{i+n-1}, k_{i+n-1})), \tag{9}$$

where η_j labels the cell (of width τ_r) containing the exit-time t_j. From the probabilities of these words one calculates the block entropies at the given time resolution, $H_n^{\Omega}(\epsilon, \tau_r)$, and then the exit-time (ϵ, τ_r)-entropies

$$h^{\Omega}(\epsilon, \tau_r) = \lim_{n\to\infty} H_{n+1}^{\Omega}(\epsilon, \tau_r) - H_n^{\Omega}(\epsilon, \tau_r). \tag{10}$$

The limit of infinite time resolution gives us the ϵ-entropy *per exit*, i.e.

$$h^{\Omega}(\epsilon) = \lim_{\tau_r\to 0} h^{\Omega}(\epsilon, \tau_r). \tag{11}$$

This result may be obtained also by arguing as follows. There is a one-to-one correspondence between the (exit-time)-histories and the (ϵ, τ)-histories (in the limit $\tau \to 0$) originating from a given ϵ-cell. The Shannon–McMillan theorem [22] assures that the number of the typical (ϵ, τ)-histories of length N, $\mathcal{N}(\epsilon, N)$, is such that: $\ln \mathcal{N}(\epsilon, N) \simeq h(\epsilon)N\tau = h(\epsilon)T$. For the number of typical (exit-time)-histories of length M, $\mathcal{M}(\epsilon, M)$, we have: $\ln \mathcal{M}(\epsilon, M) \simeq h^{\Omega}(\epsilon)M$. If we consider $T = M\langle t(\epsilon)\rangle$ we must obtain the same number of (very long) histories. Therefore, from the relation $M = T/\langle t(\epsilon)\rangle$, where $\langle t(\epsilon)\rangle = 1/M\sum_{i=1}^{M} t_i$, we obtain finally for the ϵ-entropy per unit time

$$h(\epsilon) = \frac{Mh^{\Omega}(\epsilon)}{T} = \frac{h^{\Omega}(\epsilon)}{\langle t(\epsilon)\rangle}. \tag{12}$$

Note that a relation similar to (12), without the dependence on ϵ, has been previously proposed, in the particular case of the stochastic resonance [23,24]. In such a case, where $x(t)$ effectively takes only the two values ± 1 and the transition can be assumed to be instantaneous, the meaning of the equation is rather transparent.

At this point we have to remind that in almost all practical situations there exists a minimum time interval, τ_s, a signal can be sampled with. Since there exists this minimum resolution time, we can at best estimate $h^{\Omega}(\epsilon)$ by means of $h^{\Omega}(\epsilon) = h^{\Omega}(\epsilon, \tau_s)$, instead of performing the limit (11); so that we may put

$$h(\epsilon) \simeq \frac{h^{\Omega}(\epsilon, \tau_r)}{\langle t(\epsilon)\rangle} \tag{13}$$

for small enough τ_r. In most of the cases, the leading ϵ-contribution to $h(\epsilon)$ in (13) is given by the mean exit-time $\langle t(\epsilon)\rangle$ and not by $h^{\Omega}(\epsilon, \tau_r)$. Anyhow, the computation of $h^{\Omega}(\epsilon, \tau_r)$ is compulsory in order to recover, e.g., a zero entropy for regular (e.g., periodic) signals.

Now we discuss how one can estimate the ϵ-entropy in practice. In particular, we introduce upper and lower bounds for $h(\epsilon)$ which are very easy to compute in the exit-time scheme [18]. We use the following notation: for given ϵ and τ_r, $h^{\Omega}(\epsilon, \tau_r) \equiv h^{\Omega}(\{\eta_i, k_i\})$, and we indicate with $h^{\Omega}(\{k_i\})$ and $h^{\Omega}(\{\eta_i\})$, respectively, the Shannon-entropy of the sequence $\{k_i\}$ and $\{\eta_i\}$. By applying standard results of information theory [4,5] one obtains:

1. $h^{\Omega}(\{k_i\}) \le h^{\Omega}(\{\eta_i, k_i\})$, since the mean uncertainty on the composed event $\{\eta_i, k_i\}$ cannot be smaller than that on a partial one $\{k_i\}$ (or $\{\eta_i\}$);
2. $h^{\Omega}(\{\eta_i, k_i\}) \le h^{\Omega}(\{\eta_i\}) + h^{\Omega}(\{k_i\})$, since the uncertainty is maximal if $\{k_i\}$ and $\{\eta_i\}$ are independent (correlations can only decrease the uncertainty).

Moreover, we observe that, for a given finite resolution τ_r, the associated sequence $\{\eta_i\}$ satisfies the bound

$$h^{\Omega}(\{\eta_i\}) \le H_1^{\Omega}(\{\eta_i\}).$$

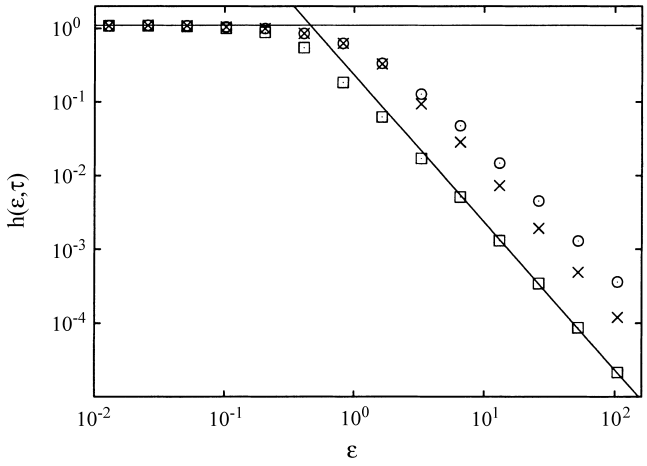

Fig. 4. Numerically computed lower (□) and upper (○) bounds (with $\tau = 1$) of $h(\epsilon)$ according to Eq. (14), for the map (6) with the same parameters as in Fig. 2. The two straight lines correspond to the asymptotic behaviours as in Fig. 2. The crosses (×) mark the values of the (ϵ, τ)-entropy $h^{\Omega}(\epsilon, \tau)/\langle t(\epsilon)\rangle$ with $\tau = 0.1\langle t(\epsilon)\rangle$.

In the above relation $H_1^{\Omega}(\{\eta_i\})$ is the one-symbol entropy of $\{\eta_i\}$ (i.e. the entropy of the probability distribution of the exit-times measured on the scale τ_r) which can be written as

$$H_1^{\Omega}(\{\eta_i\}) = c(\epsilon) + \ln\left(\frac{\langle t(\epsilon)\rangle}{\tau_r}\right),$$

where $c(\epsilon) = -\int P(z)\ln P(z)\,dz$, and $P(z)$ is the probability distribution function of the rescaled exit-time $z(\epsilon) = t(\epsilon)/\langle t(\epsilon)\rangle$. Finally, using the previous relations, one obtains the following bounds for the ϵ-entropy:

$$\frac{h^{\Omega}(\{k_i\})}{\langle t(\epsilon)\rangle} \le h(\epsilon) \le \frac{h^{\Omega}(\{k_i\}) + c(\epsilon) + \ln(\langle t(\epsilon)\rangle/\tau_r)}{\langle t(\epsilon)\rangle}. \tag{14}$$

Note that such bounds are relatively easy to compute and give a good estimate of $h(\epsilon)$. Eqs. (12)–(14) allow for a remarkable improvement of the computational efficiency. Especially as far as the scaling behaviour of $h(\epsilon)$ is concerned, one can see that the leading contribution is given by $\langle t(\epsilon)\rangle$, and that $h^{\Omega}(\epsilon, \tau_r)$ introduces, at worst, a sub-leading logarithmic contribution $h^{\Omega}(\epsilon, \tau_r) \sim \ln(\langle t(\epsilon)\rangle/\tau_r)$ (see Eq. (14)). This fact is evident in the case of Brownian motion. In this case one has $\langle t(\epsilon)\rangle \propto \epsilon^2/D$, and

1. $c(\epsilon)$ is of O(1) and independent of ϵ (since the Brownian motion is a self-affine process);
2. $h^{\Omega}(\{k_i\}) \le \ln 2$, is small compared with $\ln(\langle t(\epsilon)\rangle/\tau_r)$, so that neglecting the logarithmic corrections, $h(\epsilon) \sim 1/\langle t(\epsilon)\rangle \propto D\epsilon^{-2}$.

In Fig. 4 we show the numerical evaluation of the bounds (14) for the diffusive map (6). Fig. 4 has to be compared with Fig. 2, where the usual approach has been used. While in Fig. 2, the expected ϵ-entropy scaling is just poorly recovered as an envelope over many different τ, within the exit-time method the predicted behaviour is easily recovered in all the range of $\epsilon > 1$ with a remarkable improvement in the quality of the result.

Since we code the original W-words of length n into Ω-words of non-constant length, our approach is similar to the Ziv–Lempel compression method [3]. A similar idea has also been exploited in symbolic dynamics of intermittent maps [25,26].

We underline that the reason for which the exit-time approach is more efficient than the usual one is a posteriori intuitive. Indeed, at fixed ϵ, $\langle t(\epsilon)\rangle$ automatically gives the typical time at that scale, and, as a consequence, it is not

necessary to reach very large block sizes — at least if ϵ is not too small. Especially for large ϵ, we found that small word lengths are enough to estimate the ϵ-entropy accurately. Of course, for small ϵ (i.e. the plateau of Fig. 4) one has to use larger block sizes: here the exit-time is O(1) and one falls back to the problems of the standard method. For small ϵ in deterministic system one has to distinguish two situations:

1. $\epsilon \to 0$ for discrete-time systems. In this limit the exit-time approach coincides with the usual one. The exit-times always coincide with the minimum sampling time, i.e. $\langle t(\epsilon \to 0)\rangle \sim 1$ and we have to consider the possibility to have jumps over more than one cell, i.e. the k_i symbols may take values $\pm 1, \pm 2, \ldots$
2. $\epsilon \to 0$ for continuous-time systems. At very small ϵ, due to the deterministic character of the system, one has $\langle t(\epsilon)\rangle \sim \epsilon$, and therefore one finds words composed with highly correlated symbols. So one has to treat very large blocks in computing the entropy [27].

However, as far as high-dimensional systems are concerned, for some aspects, the points (1) and (2) are not of practical interest. In these systems the analysis of the $\epsilon \to 0$ limit is usually unattainable for several reasons [8,11], and, moreover, in many cases one is more interested in the large ϵ scale behaviour. We believe that in these cases the approach presented here, is practically unavoidable.

We conclude this section with two further remarks. First, up to now we considered a scalar signal as the output of a one-dimensional system. This fact only entered in the two-valuedness of the k-variable. If we are given a vectorial signal $\mathbf{x}(t)$, describing the evolution of a d-dimensional system, we have only to admit $2d$ values for the direction-of-exit variable k. If the dynamics is discrete one has also to consider the possibility of jumps over more than one cell (see previous discussion). Second, one can wonder about the dependence of $h(\epsilon)$ on the used observable. Rigorous results insure that the KS-entropy, i.e. the limit $\epsilon \to 0$ of $h(\epsilon)$ is an intrinsic quantity of the considered system, its value does not change under a smooth change of variables. In the case of (ϵ, τ)-entropy, in principle there could be dependencies on the chosen function. However, one can see that at least the scaling properties should not strongly depend on the choice of the observable. If $A(x)$ is a smooth function of x, such that the following property holds:

$$c_1|\delta x| \leq |A(x + \delta x) - A(x)| \leq c_2|\delta x| \tag{15}$$

with c_1 and c_2 are finite constants, then there exist two constants α_1 and α_2 such that

$$h_x\left(\frac{\epsilon}{\alpha_1}, \tau\right) \leq h_A(\epsilon, \tau) \leq h_x\left(\frac{\epsilon}{\alpha_2}, \tau\right), \tag{16}$$

where $h_A(\epsilon, \tau)$ and $h_x(\epsilon, \tau)$ are the (ϵ, τ)-entropies computed using the observable A and x, respectively. This result implies that if $h(\epsilon, \tau)$ shows a power-law behaviour as a function of ϵ, $h(\epsilon, \tau) \sim \epsilon^{-\beta}$, the same behaviour, with the same exponent β, must be seen when using another, smooth, observable in the determination of the (ϵ, τ)-entropy.

4. Application of the ϵ-entropy to deterministic and stochastic processes

4.1. An intermittent deterministic mapping

We discuss the application of exit-time approach to the computation of ϵ-entropy in strongly intermittent low-dimensional systems.

In the presence of intermittency, the dynamics is characterized by very long, almost quiescent (laminar) intervals separating short intervals of very intense (bursting) activity (see Fig. 5). Already at a qualitative level, one realizes that coding the trajectory shown in Fig. 5 at fixed sampling times (Section 2) is not very efficient compared with

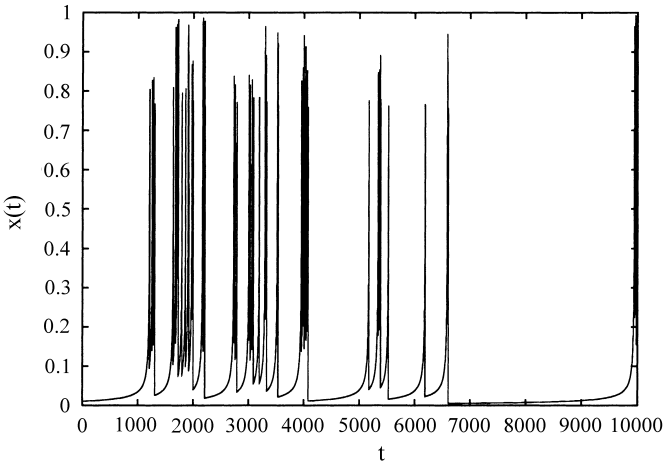

Fig. 5. Typical evolution of the intermittent map (17) for $z = 2.5$ and $a = 0.5$.

the exit-times method, where the information on the very long quiescent periods is typically stored using only one symbol. To be more quantitative, let us consider the following one-dimensional intermittent map [28]:

$$x_{t+1} = (x_t + a x_t^z) \bmod 1 \tag{17}$$

with $z > 1$ and $a > 0$. The invariant density is characterized by a power-law singularity near $x = 0$, which is a marginally stable fixed point, i.e. $\rho(x) \propto x^{1-z}$. For $z \geq 2$, the density is not normalizable, and an interesting dynamical regime, the so-called *sporadic chaos*, appears [29,30]. Namely, for $z \geq 2$ the separation between two close trajectories behaves as

$$|\delta x_n| \sim \delta x_0 \exp[c n^{\nu_0} (\ln n)^{\nu_1}] \tag{18}$$

with $0 < \nu_0 < 1$ or $\nu_0 = 1$ and $\nu_1 < 0$. In the sporadic chaos regime, nearby trajectories diverge with a stretched exponential, even if the Lyapunov exponent is zero. For $z < 2$ the system follows the usual chaotic motion with $\nu_0 = 1$ and $\nu_1 = 0$. Sporadic chaos is intermediate between chaotic motion and regular one. This can be understood by computing the Kolmogorov–Chaitin–Solomonoff complexity [29,30], or, as we show in the following, by studying the mean exit-time. By neglecting the contribution of $h^{\Omega}(\epsilon)$, and considering only the mean exit-time, we can estimate the total entropy, H_N, of a trajectory of length N as

$$H_N \propto \frac{N}{\langle t(\epsilon)\rangle_N} \quad \text{for large } N, \tag{19}$$

where $\langle [\dots] \rangle_N$ indicates that the mean exit-time is computed on a sequence of length N. Due to the power-law singularity at $x = 0$, $\langle t(\epsilon)\rangle_N$ depends on N. In Eq. (19), we have dropped from H_N the dependence on ϵ, which is expected to be weak. Indeed, due to singularity near the origin, one has that the exit-times at scale ϵ are dominated by the first exit from a region of size ϵ around the origin, so that $\langle t(\epsilon)\rangle_N$ approximately gives the duration of the laminar period (this is exact for ϵ large enough).

In Fig. 6, the behaviour of $\langle t(\epsilon)\rangle_N$ is shown as a function of N and z for two different choices of ϵ. For large enough N the behaviour is almost independent of ϵ, and for $z \geq 2$ one has

$$\langle t(\epsilon)\rangle_N \propto N^{\alpha}, \quad \text{where } \alpha = \frac{z-2}{z-1}. \tag{20}$$

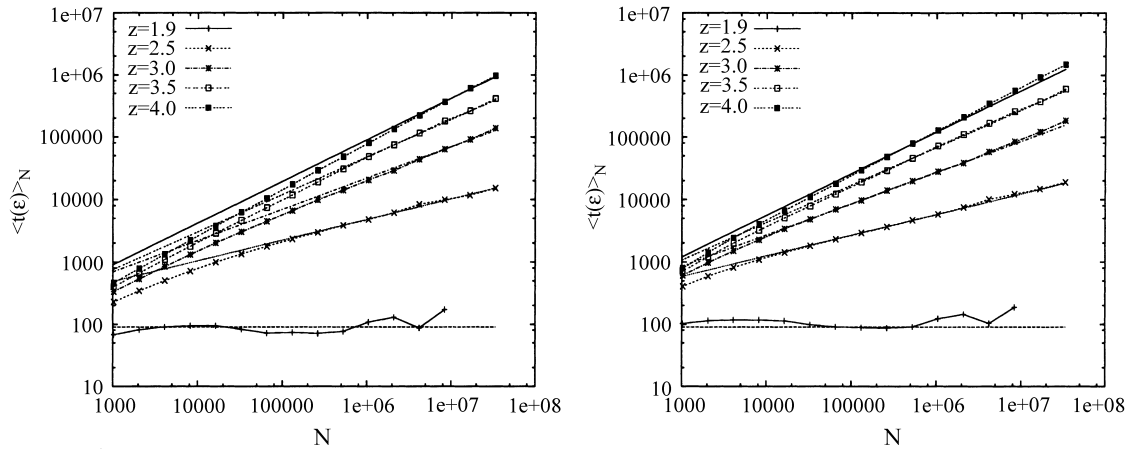

Fig. 6. $\langle t(\epsilon)\rangle_N$ versus N for the intermittent map (17) at $\epsilon = 0.001$ (left) and $\epsilon = 0.243$ (right) for different z and $a = 0.5$. The straight lines indicate the power law (20). The average $\langle t(\epsilon)\rangle_N$ has been obtained by averaging over 10^4 different trajectories of length N, this average is necessary because of the poor statistics caused by the singularity near the origin. For $z < 2$, $\langle t(\epsilon)\rangle_N$ does not depend on N, $\rho(x)$ is normalisable, the motion is chaotic and H_N/N is constant.

For $z < 2$ one has $\langle t(\epsilon)\rangle \approx$ constant at large N. The value of α is obtained by the following argument: the power-law singularity leads to $x_t \approx 0$ most of the time, and moreover, near the origin the map (18) can be approximated by the differential equation $\mathrm{d}x/\mathrm{d}t = ax^z$ [28]. Therefore, denoting with x_0 the initial condition, one solves the differential equation obtaining

$$(x_0 + \epsilon)^{1-z} - x_0^{1-z} = a(1-z)t(\epsilon).$$

Now, due to the singularity, x_0 is typically much smaller than $x_0 + \epsilon$, and hence we can neglect the term $(x_0+\epsilon)^{1-z}$, so that the exit-time is $t(\epsilon) \propto x_0^{1-z}$. By the probability density of x_0, $\rho(x_0) \propto x_0^{1-z}$, one obtains the probability distribution of the exit-times $\rho(t) \sim t^{1/(1-z)-1}$, the factor t^{-1} takes into account the non-uniform sampling of the exit-time statistics (see discussion after Eq. (25)). Finally the average exit-time on a trajectory of length N, which is given by

$$\langle t(\epsilon)\rangle_N \sim \int_0^N t\rho(t)\,\mathrm{d}t \sim N^{(z-2)/(z-1)}. \tag{21}$$

The total entropy is finally given by

$$H_N \sim \frac{N}{N^{(z-2)/(z-1)}} \sim N^{1/(z-1)},$$

note that this is exactly the same N-dependence found with the computation of the algorithmic complexity [29,30]. Let us underline that the entropy per unit time goes to zero very slowly, because of the sporadicity

$$\frac{H_N}{N} \sim \frac{1}{\langle t(\epsilon)\rangle_N}.$$

Let us note that we arrive at this results without any partitions of the phase-space of the system.

4.2. Affine and multi-affine stochastic processes

Self- and multi-affine processes are fully characterized by the scaling laws of the moments of signal increments [14,31,32], $\delta_t x = x(t_0) - x(t_0 + t)$:

$$\langle\langle |\delta_t x(t_0)|^q \rangle\rangle \sim t^{\zeta(q)}, \tag{22}$$

where $\zeta(q)$ is a linear function of q, $\zeta(q) = \xi q$, for a self-affine signal (ξ is the Hölder exponent characterizing the process) and a non-linear function of q for a multi-affine signal. The average $\langle\langle\cdot\rangle\rangle$ is defined as the average over the process distribution $P(t_0, \delta_t x(t_0))$, which gives the probability to have a fluctuation, $\delta_t x(t_0)$, at the instant t_0. In the case of a stationary process, as it will be always assumed here, the probability distribution is time invariant and the average $\langle\langle\cdot\rangle\rangle$ is computed by invoking an ergodic hypothesis, as a time-average. Sometimes, with an abuse of language, a multi-affine process is also called a multifractal process. While a self-affine process has a global scaling-invariant probability distribution function, a multi-affine process can be constructed by requiring a local (in time) scaling-invariant fluctuations [14]. In a nutshell, one assumes a spectrum of different local scaling exponents ξ: $\delta_t x(t_0) \sim t^{\xi(t_0)}$ with the probability $P_t(\xi) \sim t^{1-D(\xi)}$ to observe a given Hölder exponent ξ at time increment t. The function $D(\xi)$ can be interpreted as the fractal dimension of the set where the Hölder exponent ξ is observed [31]. The scaling exponents $\zeta(q)$ are related to $D(\xi)$ by a Legendre transform. Indeed, one may define the average process as an average over all possible singularities, ξ, weighted by the probability to observe them:

$$\langle\langle (\delta_t x)^q \rangle\rangle \sim \int \mathrm{d}\xi\, t^{\xi q} t^{1-D(\xi)},$$

which in the limit of small t by a saddle point estimation becomes

$$\langle\langle (\delta_t x)^q \rangle\rangle \sim t^{\zeta(q)} \quad \text{with} \quad \zeta(q) = \min_{\xi}(q\xi + 1 - D(\xi)). \tag{23}$$

Eq. (23) can be generalized to $\zeta(q) = \min_{\xi}(q\xi + d - D(\xi))$ if the considered signal is embedded in a d-dimensional space. Let us notice that in this language, the already discussed Brownian motion corresponds to a self-affine signal with only one possible exponent $\xi = \frac{1}{2}$ with $D(\frac{1}{2}) = 1$. In Appendix A one finds how to construct arbitrary self- and multi-affine stochastic processes.

Let us now investigate the ϵ-entropy properties of these two important classes of stochastic signals by using the exit-time approach. We will proceed by discussing the general case of multi-affine processes, noting that the self-affine one is a particular case of them corresponding to have only one exponent in the spectrum. The exit-time probability distribution function can be guessed by "inverting" the multifractal probability distribution functions [33]. We expect that the following dimensional inversion should be correct (at least as far as leading scaling properties are concerned). We argue that the probability to observe an exit of the signal through a barrier of height δx in a time $t(\delta x)$ is given by $P_{\delta x}(t(\delta x)) \sim (\delta x)^{(1-D(\xi))/\xi}$, where the height of the barrier and the exit-time are related by the inversion of the previously introduced multi-affine scaling relation $t(\delta x) \sim (\delta x)^{1/\xi}$. In this framework we may write down the "multifractal" estimate [33] of the exit-time moments, also called inverse structure functions [34]:

$$\Sigma_q(\delta x) \equiv \langle\langle t^q(\delta x)\rangle\rangle \sim \int \mathrm{d}\xi (\delta x)^{(q+1-D(\xi))/\xi} \sim (\delta x)^{\chi(q)}, \tag{24}$$

where $\chi(q)$ is obtained with a saddle point estimate in the limit of small δx:

$$\chi(q) = \min_{\xi}\left(\frac{q + 1 - D(\xi)}{\xi}\right). \tag{25}$$

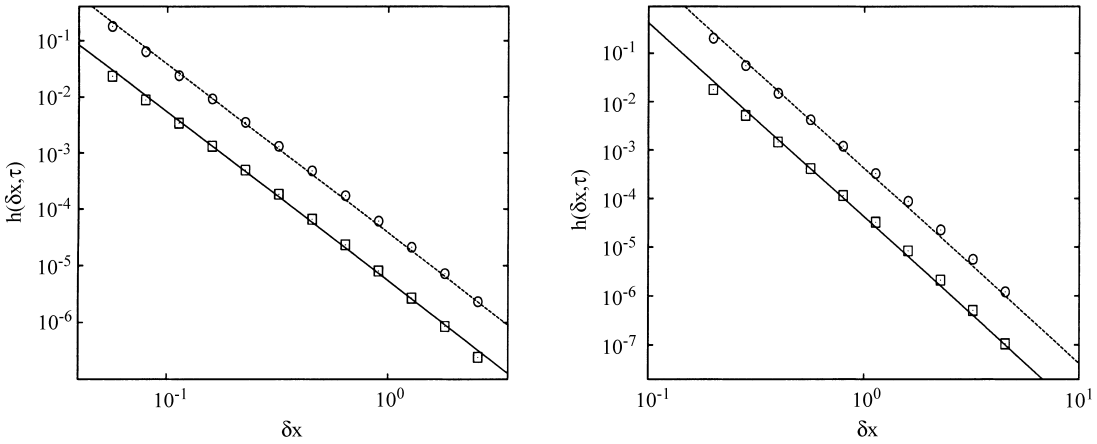

Fig. 7. Numerically computed lower (□) and upper (○) bounds for the (ϵ, τ)-entropy in the case of a self-affine signal with $\xi = \frac{1}{3}$ (left) and $\frac{1}{4}$ (right), with $\tau = 0.1\langle t(\epsilon)\rangle$. The two straight lines show the scaling ϵ^{-3} and ϵ^{-4} for the left and the right figure, respectively.

The averaging by counting the number of exit-time events M (as we did in the previous sections) and the averaging with the uniform "multifractal" distribution are connected by the following relation [33]:

$$\langle\langle t^q(\delta x)\rangle\rangle = \lim_{M\to\infty}\sum_{i=1}^{M} t_i^q \frac{t_i}{\sum_{j=1}^{M} t_j} = \frac{\langle t^{q+1}(\delta x)\rangle}{\langle t(\delta x)\rangle},$$

where the term $t_i/\sum_{j=1}^{M} t_j$ takes into account the non-uniformity of the exit-time statistics. From the previous relation evaluated for $q = -1$ we can easily deduce the estimate for the mean exit-time scaling law:

$$\langle t(\delta x)\rangle = \langle\langle t^{-1}(\delta x)\rangle\rangle^{-1} \sim (\delta x)^{-\chi(-1)} \tag{26}$$

and therefore, as in the previous sections, we may estimate the leading contribution to the ϵ-entropy of a multi-affine signal:

$$h(\delta x) \sim (\delta x)^{\chi(-1)}. \tag{27}$$

Let us notice that in the simpler case of a self-affine signal with Hölder exponent ξ, this is nothing but the dimensional estimate $h(\delta x) \sim (\delta x)^{-1/\xi}$ which is rigorous for Gaussian processes [16,17]. In this case the above argument is also in agreement with the bounds (14): indeed for an affine signal the function $c(\epsilon)$ entering in (14) does not depend on ϵ (we note here that δx plays the same role of ϵ).

In Fig. 7a and b, we show the numerical estimate of the bounds (14) on the ϵ-entropy in two different self-affine signals with Hölder exponents $\xi = \frac{1}{3}$ and $\frac{1}{4}$, respectively (for details on the processes generation, see Appendix A). The agreement with the expected result is very good. Let us notice that with the usual approach to the calculation of the ϵ-entropy for these simple signals the detection of the scaling behaviour is not so easy (see Figs. 15–17 of [8]).

In Fig. 8 we show the numerically computed lower and upper bounds for the ϵ-entropy of a multi-affine signal by using the mean exit-time estimate. The multi-affine signal here studied is characterized by having $\zeta(q)$ as the scaling exponent measured in turbulence (see Section 5). In particular, this means that $\zeta(3) = 1$, and using Eqs. (23) and (25) $\chi(-1) = -3$ independently on the shape of $D(\xi)$. This is the ϵ-entropies counterpart of the Kolmogorov $4/5$ law [14]. The agreement with the multifractal prediction (the straight lines in Fig. 8) is impressive. To our knowledge this is the first direct estimate of ϵ-entropy in multi-affine signals. We stress that the non-trivial aspect of such an estimate is contained in the derivation of the inverse multifractal formulas (24) and (25).

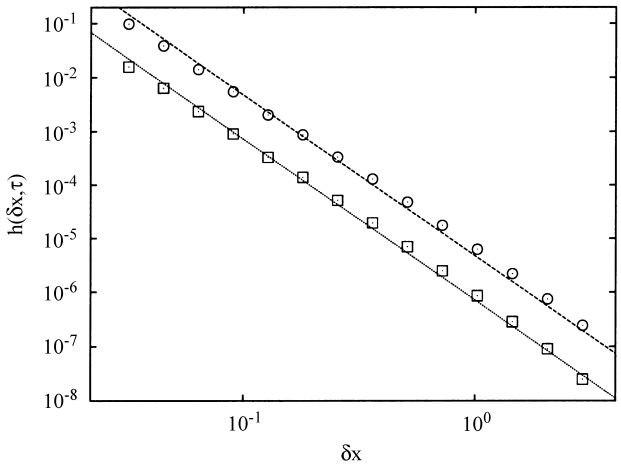

Fig. 8. Numerically computed lower (□) and upper (○) bounds, with $\tau = 0.1\langle t(\epsilon)\rangle$ for the (ϵ, τ)-entropy in the case of a multi-affine signal with $\zeta(3) = 1$. The signal has been obtained with the method of Ref. [45] (see also Appendix A) using a $D(\xi)$ which fits experimental data at large Reynolds number. The two straight lines show the theoretical scaling ϵ^{-3}.

5. ϵ-entropy and exit-times in turbulence

A turbulent flow is characterized by the presence of highly non-trivial chaotic fluctuations in space and time [14]. The question we want to address here is to understand which kind of information can be captured by studying the ϵ-entropy of this important high-dimensional dynamical system. The main physical mechanism is the energy transfer from large scales, L_0, i.e. scales where forcing is active, down to the dissipation scale, η, where kinetic energy is converted into heat [14,32]. The ratio between these two scales increases with the Reynolds number. Fully developed turbulence corresponds to the limit of very high-Reynolds numbers. In this limit, a turbulent velocity field develops scaling laws in the range of scale intermediate between L_0 and η, the so-called inertial range. Kolmogorov theory (1941) assumes a perfect self-similar behaviour for the velocity field in the inertial range. In other words, the velocity field was thought to be a continuous self-affine field with Hölder exponent $\xi = \frac{1}{3}$ as a function of its spatial coordinates:

$$|v(x + R, t) - v(x, t)| \sim R^{1/3}$$

(hereafter, for simplicity, we neglect the vectorial notation). In terms of an averaged observable, this implies that the structure functions, i.e. the moments of simultaneous velocity differences at distance R, have a pure power-law dependency for $\eta \ll R \ll L_0$

$$S_p(R) = \langle\langle |v(x + R, t) - v(x, t)|^p \rangle\rangle \sim R^{\zeta(p)} \tag{28}$$

with $\zeta(p) = \frac{1}{3}p$. Experiments and numerical simulations have indeed shown that there are small (but important) corrections to the Kolmogorov prediction (1941). This problem goes under the name of intermittency, the origin of which is still one of the main open problem in the theory of Navier–Stokes equations [14,32,35,36]. In the language of the previous section, an intermittent field is a multi-affine process.

As far as the time-dependency of a turbulent velocity field is concerned, one can distinguish between two different time measurements. First, the standard one (actually used in most of the experimental investigation), consists in measuring the time evolution by a probe fixed in some spatial location, say x_p, in the flow. The time evolution obtained in this way is strongly affected by the spatial correlations induced by the large scales sweeping. As a

result, one can apply the so-called frozen-turbulent hypothesis (Taylor hypothesis) [35,36], which connects a time measurement with a spatial measurement by the following relation:

$$v(x_p, t_0 + t) - v(x_p, t_0) \sim v(x_p - R, t_0) - v(x_p, t_0),$$

where $R = tU_0$ and U_0 is the mean large scale sweeping velocity characteristic of the experiment. As a result of the Taylor-hypothesis, one has that time measurements also show power-law behaviour with the same characteristic exponents of the spatial measurements, namely, within the Kolmogorov theory

$$\langle\langle |v(x_p, t_0 + t) - v(x_p, t_0)|^p \rangle\rangle \sim t^{\zeta(p)}.$$

A second interesting possibility to perform time measurements consists in the so-called Lagrangian measurements [37]. In this case, one has to follow the trajectory of a single fluid particle and measuring the time properties locally in the co-moving reference frame. The main characteristics of this method is that the sweeping is removed and so one can probe in details the "proper" time-fluctuations induced by the nonlinear terms of the Navier–Stokes equations (for recent theoretical and numerical investigations of similar issues, see [37–40]).

The phenomenological understanding of all these spatial and temporal properties are well summarized by the Richardson-cascade. The cascade picture describes a turbulent flow in terms of a superposition of fluctuations (eddies) hierarchically organized on a set of scales ranging from the largest one, L_0, to the smallest one, η, say $\ell_n = 2^{-n} L_0$ with $n = 0, \ldots, N_{\max}$ and $N_{\max} = \log_2(L_0/\eta)$. Each scale has its own typical evolution time, τ_n, given in terms of the velocity difference at that scale, $\delta_n v = v(x + \ell_n) - v(x)$, by the dimensional estimate: $\tau_n = \ell_n/\delta_n v \sim (\ell_n)^{2/3}$. The most relevant dynamical interactions are supposed to happen only between eddies of similar size, while each eddy is also subject to the spatial sweeping from eddies at larger scales. The energy is transferred down-scale from the largest-eddy (the mother) to its daughters and from the daughters to their grand-daughters and so on in a multi-step process similar, quantitatively and qualitatively to a stochastic multiplicative process [41,42].

As a result of the previous picture, one can mimic a turbulent flow with a stochastic process hierarchically organized in space, and with suitable time-dependence able to reproduce both the overall sweeping and the eddy-turn-over times hierarchy [43–45]. In Appendices A and B, we briefly remind a possible choice for these stochastic process.

5.1. Experimental data analysis

Now we present the computation of the ϵ-entropy for two sets of high-Reynolds number experimental data, obtained from an experiment in Lyon (at $Re_\lambda = 400$) and from another experiment in Modane (at $Re_\lambda = 2000$). The measurement in Lyon has been taken in a wind tunnel with a working section of 3.0 m and a cross section of $0.5 \times 0.5\,\mathrm{m}^2$. Turbulence was generated by a cylinder placed inside the wind tunnel, its diameter was 0.1 m. The hot wire was placed 2.0 m behind the cylinder. The separation between both probes was approximately 1 mm [51]. The measurement in Modane has been taken in a wind tunnel where the integral scale was $L \sim 20$ m and the dissipative scale was $r_{\mathrm{diss}} = 0.3$ mm.

Let us first make an important remark. Whenever one wants to apply the multifractal formalism to turbulence there exist some analytical and phenomenological constraints on the shape of the function $D(\xi)$ entering in the multifractal description. In particular, the most important constraint is the exact result $\zeta(3) = 1$. This, in turn, implies that independently of the possible multifractal spectrum of the turbulent field one has $\chi(-1) = -3$, so that as stated in the previous section, one obtains

$$h(\epsilon) \sim \epsilon^{\chi(-1)} = \epsilon^{-3}, \tag{29}$$

this is the ϵ-entropy equivalent of the $\zeta(3) = 1$ result, i.e. of the 4/5 law of turbulence [14] (see Eqs. (26) and (27)). This means that there are no intermittent corrections to the ϵ-entropy. We have tested this prediction (here for the

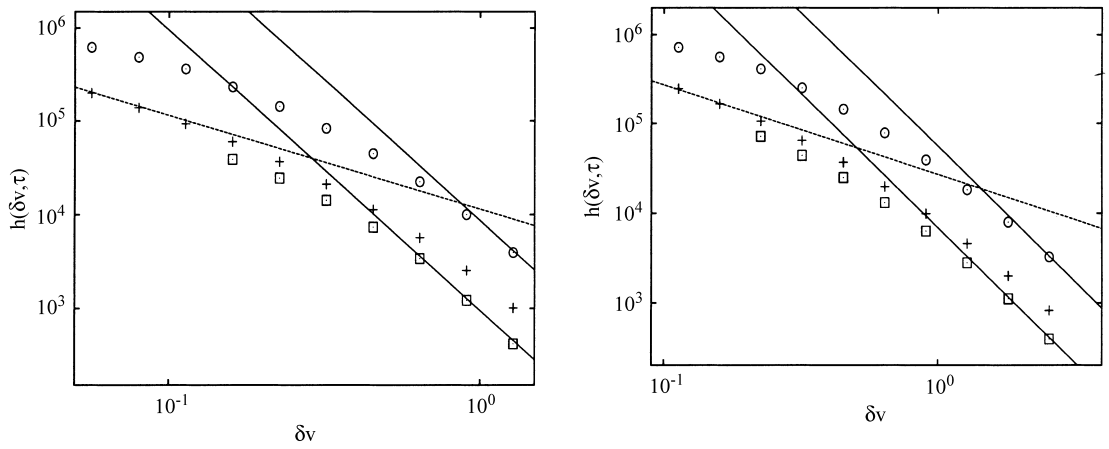

Fig. 9. Numerically computed lower (□) and upper (○) bounds, with $\tau = 0.1\langle t(\epsilon)\rangle$ for the (ϵ, τ)-entropy in the case of Lyon turbulent data (left) and Modane turbulent data (right). We also show $\langle t(\delta v)\rangle^{-1}$ (+) and its trivial dissipative scaling δv^{-1} (dashed line). The full line follows the scaling δv^{-3} for the ϵ-entropy, as predicted in Eq. (29).

first time presented), which has been already confirmed in the analysis of the stochastic multi-affine signal in Section 4.2, in two different experimental data sets. In Fig. 9 we show the ϵ-entropy computed for two different sets of experimental data. As one can see, the theoretical prediction $h(\epsilon) \sim \epsilon^{-3}$ is well reproduced only for large ϵ values, while for intermediate values the entropy shows a continuous bending without any clear scaling behaviour, only when ϵ reaches values corresponding to dissipative velocity fluctuations we have the dissipative scaling $\langle t(\epsilon)\rangle \sim \epsilon$. The strong intermediate regime between the dissipative and the inertial scaling behaviours is not a simple out-of-control finite Reynolds effect. In fact, within the multifractal model of turbulence, one can understand the large crossover between the two power laws in terms of the so-called intermediate-dissipative-range (IDR). The existence of an IDR was originally predicted in [46] and further analysed in [33,47,48]. The IDR brings the signature of the mechanism stopping the turbulent energy cascade, i.e. how viscous mechanism are effective in dissipating turbulent energy. In particular, it was shown that the IDR can be fully described within the multifractal description once one allows the possibility to have different viscous cut-off depending on the local degree of velocity singularity, i.e. depending on the local realization of the ξ scaling exponent. The main idea consists in using again the multifractal superposition (24) but considering that for velocity fluctuations at the edge between the inertial and the viscous range not all possible scaling exponents contribute to the average [33,46]. It turns out that in the case of exit-time moments, the extension of the IDR is much more important then what was previously measured for the velocity structure functions (28). Therefore, the strong finite-range effects showed by the experimental data analysis of Fig. 9 can be qualitatively and quantitatively understood as an effect of the IDR [33].

Let us conclude this section by comparing our results with a previous study of the ϵ-entropy in turbulence [15]. There it was argued the following scaling behaviour:

$$h(\epsilon) \sim \epsilon^{-2}, \tag{30}$$

which differs from our prediction. The behaviour (30) has been obtained assuming that $h(\epsilon)$ at scale ϵ is proportional to the inverse of the typical eddy-turn-over time at that scale. We remind that here ϵ represents a velocity fluctuation δv. Since the typical eddy-turn-over time for velocity fluctuations of order $\delta v \sim \epsilon$ is $\tau(\epsilon) \sim \epsilon^2$, Eq. (30) follows. Recalling the discussion of Section 5.1 about the two possible way of measuring a turbulent time signal it is clear that the scaling (30) holds only in a Lagrangian reference frame (see also [9,10]). This explains the difference of our prediction and (30).

5.2. An ϵ-entropy analysis of the Taylor hypothesis in fully developed turbulence

By studying the ϵ-entropy for the velocity field of turbulent flows in $3+1$ dimension, $h^{\mathrm{st}}(\epsilon)$ (st indicates *space* and *time*), we argue that the usually accepted Taylor hypothesis implies a spatial correlation which can be quantitatively characterized by an "entropy" dimension $\mathcal{D} = \frac{8}{3}$. In this section, for the sake of simplicity, we neglect intermittency, i.e. we assume a pure self-affine field with Hölder exponent $\xi = \frac{1}{3}$.

We discuss now how to construct a multi-affine field with the proper spatial and temporal scaling. The idea consists in defining the signal as a dyadic three-dimensional superposition of wavelet-like functions $\varphi((\mathbf{x} - \mathbf{x}_{n,k}(t))/\ell_n)$ whose centres move according to a swept dynamics. The coefficients of the decomposition $a_{n,k}(t)$ are stochastic functions chosen with suitable self-affine scaling properties both in time and in space. In particular, the exact definition for a field with spatial Hölder exponent ξ in d dimensions is (see Appendix A for a brief review of some existing results on synthetic turbulence, and Appendix B for a generalization which includes sweeping effects in order to consider in a proper way the spatio-temporal correlations)

$$v(\mathbf{x}, t) = \sum_{n=1}^{M} \sum_{k=1}^{2^{d(n-1)}} a_{n,k}(t)\, \varphi\left(\frac{\mathbf{x} - \mathbf{x}_{n,k}(t)}{\ell_n}\right), \tag{31}$$

where $\mathbf{x}_{n,k}$ is the centre of the kth wavelets at the level n (for each dimension we consider one branching, i.e. two variables, for passing to the $n+1$ level, see Fig. 10). According to the Richardson–Kolmogorov cascade picture, one assumes that sweeping is present, i.e. $\mathbf{x}_{n+1,k} = \mathbf{x}_{n,k'} + \mathbf{r}_{n+1,k}$, where (n, k') labels the "mother" of the $(n+1, k)$-eddy and $\mathbf{r}_{n+1,k}$ is a stochastic vector which depends on $\mathbf{r}_{n,k'}$ and evolves with characteristic time $\tau_n \propto (\ell_n)^{1-\xi}$. If the coefficients $\{a_{n,k}\}$ and $\{\mathbf{r}_{n,k}\}$ have characteristic time $\tau_n \sim (\ell_n)^{1-\xi}$ and $\{a_{n,k}\} \sim (\ell_n)^{\xi}$, it is possible to show (see Appendices A and B for details) that the field (31) has the properties

$$|v(\mathbf{x} + \mathbf{R}, t_0) - v(\mathbf{x}, t_0)| \sim |\mathbf{R}|^{\xi}, \tag{32}$$

$$|v(\mathbf{x}, t_0 + t) - v(\mathbf{x}, t_0)| \sim t^{\xi}, \tag{33}$$

in addition the proper Lagrangian sweeping is satisfied. Now we are ready for the ϵ-entropy analysis of the field (31). If one wants to look at the field v with a resolution ϵ, one has to take n up to N given by

$$(\ell_N)^{\xi} \sim \epsilon, \tag{34}$$

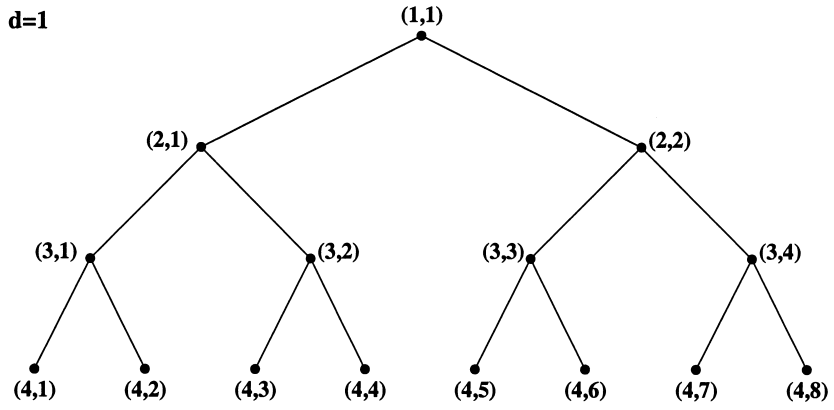

Fig. 10. Branching process for the multiplicative model (we only show the $d = 1$ case), as described in the main text.

in this way we are sure to consider velocity fluctuations of order ϵ. Then the number of terms contributing to (31) is

$$\#(\epsilon) \sim (2^d)^N \sim \epsilon^{-d/\xi}. \tag{35}$$

By using a result of Shannon [4,5] one estimates the ϵ-entropy of the process $a_{n,k}(t)$ (and also of $\mathbf{r}_{n,j}$) as

$$h_n(\epsilon) \sim \frac{1}{\tau_n} \log\left(\frac{1}{\epsilon}\right), \tag{36}$$

where the above relation is rigorous if the processes $a_{n,k}(t)$ are Gaussian and with a power spectrum different form zero on a band of frequency $\sim 1/\tau_n$. The terms which give the main contribution are those with $n \sim N$ with $\tau_N \sim (\ell_N)^{1-\xi} \sim \epsilon^{(1-\xi)/\xi}$. Collecting the above results, one finds

$$h^{\mathrm{st}}(\epsilon) \sim \frac{\#(\epsilon)}{\tau_N} \sim \epsilon^{-(d-\xi+1)/\xi}. \tag{37}$$

For the physical case $d = 3$, $\xi = \frac{1}{3}$, one obtains

$$h^{\mathrm{st}}(\epsilon) \sim \epsilon^{-11}. \tag{38}$$

The above result, has already been obtained in [8] with a different consideration. By denoting with v_k the typical velocity at the Kolmogorov scale η, one has that Eq. (38) holds in the inertial range, i.e. $\epsilon \geq v_k \sim Re^{-1/4}$, while for $\epsilon \leq v_k$, $h^{\mathrm{st}}(\epsilon) = \text{constant} \sim Re^{11/4}$. Let us now discuss the physical implications of (37). Consider an alternative way to compute the ϵ-entropy of the field $v(\mathbf{x}, t)$: divide the d-volume in boxes of edge length $\ell(\epsilon) \sim \epsilon^{1/\xi}$ and look at the signals $v(\mathbf{x}_\alpha, t)$, where the $\mathbf{x}_\alpha$ are the centres of the boxes. In each $\mathbf{x}_\alpha$, we have a time record whose ϵ-entropy is

$$h^{(\alpha)}(\epsilon) \sim \epsilon^{-1/\xi} \tag{39}$$

because of the scaling (33). In (39) we use the symbol $h^{(\alpha)}$ to denote the entropy of the temporal evolution of the velocity field measured in $\mathbf{x}_\alpha$. Therefore, $h^{\mathrm{st}}(\epsilon)$ will be obtained summing up all the "independent" contributions (39), i.e.

$$h^{\mathrm{st}}(\epsilon) \sim \mathcal{N}(\epsilon) h^{(\alpha)}(\epsilon) \sim \mathcal{N}(\epsilon)\epsilon^{-1/\xi}, \tag{40}$$

where $\mathcal{N}(\epsilon)$ is the number of independent cells. It is easy to understand that the simplest assumption $\mathcal{N}(\epsilon) \sim l(\epsilon)^d \sim \epsilon^{d/\xi}$ gives a wrong result, indeed one obtains

$$h^{\mathrm{st}}(\epsilon) \sim \epsilon^{-(d+1)/\xi}, \tag{41}$$

which is not in agreement with (37). In order to obtain the correct result (38) it is necessary to assume

$$\mathcal{N}(\epsilon) \sim l(\epsilon)^{\mathcal{D}} \tag{42}$$

with $\mathcal{D} = d - \xi$. In other words, one has to consider that the sweeping implies a non-trivial spatial correlation, quantitatively measured by the exponent $\mathcal{D}$, which can be considered as a sort of "entropy" dimension. Incidentally, we note that $\mathcal{D}$ has the same numerical value as the fractal dimensions of the iso-surfaces $v = \text{constant}$ [49]. From this observation, at first glance, one could conclude that the above result is somehow trivial since it is simply related to a geometrical fact. However, a closer inspection reveals that this is not true. Indeed, one can construct a self-affine

field with spatial scaling ξ and thus with the fractal dimension of the iso-surfaces $v =$ constant given by $d - \xi$ for geometrical reasons, while $\mathcal{D} = d$. Such a process can be simply obtained by eliminating the sweeping, i.e.

$$v(\mathbf{x}, t) = \sum_{n=1}^{M} \sum_{k=1}^{2^{d(n-1)}} a_{n,k}(t)\, \varphi\left(\frac{\mathbf{x} - \mathbf{x}_{n,k}}{\ell_n}\right), \tag{43}$$

where now the $\mathbf{x}_{n,k}$ are fixed and no longer time-dependent, while $a_{n,k} \sim (\ell_n)^{\xi}$ but $\tau_n \sim \ell_n$. For a field described by (43) one has that (32) and (33) hold but $h^{\mathrm{st}}(\epsilon) \sim \epsilon^{-(d+1)/\xi}$ and $\mathcal{D} = d$, while the fractal dimension of the iso-surfaces $v =$ constant is $d - \xi$. We conclude by noting that it is possible to obtain (see [8]) the scaling (37) using Eq. (43), i.e. ignoring the sweeping, assuming $\tau_n \sim (\ell_n)^{1-\xi}$ and $a_{n,k} \sim (\ell_n)^{\xi}$, this corresponds to take separately the proper temporal and spatial spectra. However, this is not completely satisfactory since one has not the proper scaling in one fixed point (see Eq. (39) the only way to obtain this is through the sweeping).

6. Conclusion

In this paper, we have presented an investigation of deterministic mappings, stochastic processes and turbulence in terms of the ϵ-entropy. The major advantage of the ϵ-entropy with respect to the KS-entropy (or usual Lyapunov exponent) is the possibility to have information about the different temporal scales which are present in the system.

The basic idea of our approach is to look at a sequence of data, not at fixed sampling time, but only when the fluctuation in the signal is larger than some fixed threshold, ϵ. This procedure allows a remarkable improvement of the possibility to compute (ϵ, τ)-entropy, which is well represented by the exact result (12) and the bounds (14).

This approach is particularly suitable in those systems without a unique characteristic time. In such cases the method based on a coarse-grained dynamics on a fixed (ϵ, τ) grid does not work very efficiently, words of very long size being involved.

We recall that the mathematical definition of the ϵ-entropy demands consideration of the infimum over all possible partitions of the phase-space into elements with diameter not larger than ϵ [8]. Yet, in numerical investigations, one is limited for choosing a limited number of partitions and then computing the entropy with the resulting symbolic sequences. As far as the scaling behaviour of the ϵ-entropy is concerned, one expects that the chosen partition will only modify the prefactors and not the scaling exponents, at least if the system is not too inhomogeneous in the range of scales in which one is interested in.

As far as we know, there are no rigorous results concerning the dependency of the ϵ-entropy on the partitions used, and there are no explicit examples where the scaling behaviour of the ϵ-entropy is found to depend on the choice of the partition (within a reasonable class). A rigorous study of the exit-time approach for the case of strongly non-homogeneous systems and/or for systems where simple cubic partitions do not capture the correct ϵ-dependency of the ϵ-entropy (if such systems exist) is beyond the scope of the present paper.

While the computational drawbacks of standard algorithms may obscure even the ϵ-entropy scaling behaviour (see Fig. 2), we have shown that the coding in terms of the exit-time events allows for a significant improvement in detecting the scaling behaviour of the ϵ-entropy, and, moreover, in estimating its lower and upper bounds.

We have applied the method to different systems: chaotic diffusive maps, intermittent maps showing sporadic chaos, self- and multi-affine stochastic processes, and experimental turbulence data.

Applying the multifractal formalism one predicts the scaling $h(\epsilon) \sim \epsilon^{-3}$ for time measurement of velocity at a given point in turbulent flows. This power law does not depend on the intermittent corrections and has been confirmed by the experimental data analysis results. Moreover, we have shown the connection of the Taylor-frozen

hypothesis and the ϵ-entropy: the sweeping implies a non-trivial spatial correlation, quantitatively measured by an "entropy" dimension $\mathcal{D} = \frac{8}{3}$.

After the completion of our paper we became aware of Ref. [52] where an exit-time approach has been used to characterize particle motion in supercooled liquids.

Acknowledgements

We acknowledge useful discussions with G. Boffetta, A. Celani and P. Cvitanović, and the encouragement by B. Marani and F. di Carmine. We are particularly indebted to Y. Gagne and to G. Ruiz-Chavarria for having provided us with their experimental data. This work has been partially supported by INFM (PRA-TURBO) and by the European Network *Intermittency in Turbulent Systems* (contract number FMRX-CT98-0175) and the MURST *cofinanziamento* 1999 "Fisica statistica e teoria della materia condensata". M.A. is supported by the European Network *Intermittency in Turbulent Systems*.

Appendix A

In this appendix we recall some recently obtained results on the generation of multi-affine stochastic signals [43–45]. The goal is to have a stochastic process whose scaling properties are fully under control. The first step consists in generating a one-dimensional signal and the second in decorating it such as to build the most general $(d+1)$-dimensional process, $v(\mathbf{x}, t)$, with given scaling properties in time and in space. As for the simplest case of a one-dimensional system there are at least two different kind of algorithms. One is based on a dyadic decomposition of the signal in a wavelet basis with a suitable assigned series of stochastic coefficients [43,44]. The second is based on a multiplication of sequential Langevin processes with a hierarchy of different characteristic times [45]. The first procedure suits particularly appealing for the modelization of spatial turbulent fluctuations, because of the natural identification between wavelets and eddies in the physical space. The second one, on the other hand, looks more appropriate for mimicking the turbulent time evolution in a fixed point of the space, because of its sequential nature.

Let us first summarize the main ingredient of both and then briefly explain how to merge them in order to have a realistic spatial-temporal multi-affine signal. A non-sequential algorithm for one-dimensional multi-affine signal in $[0, 1]$, $v(x)$, can be defined as [43,44]

$$v(x) = \sum_{n=1}^{N} \sum_{k=1}^{2^{(n-1)}} a_{n,k}\, \varphi\left(\frac{x - x_{n,k}}{\ell_n}\right), \tag{A.1}$$

where we have introduced a set of reference scales $\ell_n = 2^{-n}$ and the function $\varphi(x)$ is a wavelet-like function [50], i.e. of zero mean and rapidly decaying in both real space and Fourier space. The signal $v(x)$ is built in terms of a superposition of fluctuations, $\varphi((x - x_{n,k})/\ell_n)$ of characteristic width ℓ_n and centred in different points of $[0, 1]$, $x_{n,k} = (2k + 1)/2^{n+1}$. In [45] it has been proved that provided the coefficients $a_{n,k}$ are chosen by a random multiplicative process, i.e. the daughter is given in terms of the mother by a random process, $a_{n+1,k'} = X a_{n,k}$ with X a random number i.i.d. for any $\{n, k\}$, then the result of the superposition is a multi-affine function with given scaling exponents, namely

$$\langle\langle |v(x + R) - v(x)|^p \rangle\rangle \sim R^{\zeta(p)}$$

with $\zeta(p) = -\frac{1}{2}p - \log_2\langle X^p\rangle$ and $\ell_N \leq R \leq 1$. In this appendix $\langle\cdot\rangle$ indicates the average over the probability distribution of the multiplicative process. Besides the rigorous proof, the rationale for the previous result is simply

that due to the hierarchical organization of the fluctuations one may easily estimate that the term dominating the expression of a velocity fluctuation at scale R, in (A.1) is given by the couple of indices $\{n, k\}$ such that $n \sim \log_2(R)$ and $x \sim x_{n,k}$, i.e. $v(x+R) - v(x) \sim a_{n,k}$. The generalization (A.1) to d-dimensional fields is given by

$$v(\mathbf{x}) = \sum_{n=1}^{N} \sum_{k=1}^{2^{d(n-1)}} a_{n,k}\, \varphi\left(\frac{\mathbf{x} - \mathbf{x}_{n,k}}{\ell_n}\right),$$

where now the coefficient $a_{n,k}$ are given in terms of a d-dimensional dyadic multiplicative process. This class of stochastic fields has been of great help in mimicking simultaneous spatial fluctuations of turbulent flows. On the other hand, as previously said, sequential algorithms look more suitable for mimicking temporal fluctuations. Let us now discuss how to construct these stochastic multi-affine fields. With the application to time-fluctuations in mind, we will denote now the stochastic one-dimensional functions with $u(t)$. The signal $u(t)$ is obtained by a superposition of functions with different characteristic times, representing eddies of various sizes [45]

$$u(t) = \sum_{n=1}^{N} u_n(t). \tag{A.2}$$

The functions $u_n(t)$ are defined by the multiplicative process

$$u_n(t) = g_n(t) x_1(t) x_2(t) \cdots x_n(t), \tag{A.3}$$

where $g_n(t)$ are independent stationary random processes, whose correlation times are supposed to be $\tau_n = (\ell_n)^\alpha$, where $\alpha = 1 - \xi$ (i.e. τ_n are the eddy-turn-over time at scale ℓ_n) in the quasi-Lagrangian reference frame [37] and $\alpha = 1$ if one considers $u(t)$ as the time signal in a given point, and $\langle g_n^2 \rangle = (\ell_n)^{2\xi}$, where ξ is the Hölder exponent. For a signal mimicking a turbulent flow, ignoring intermittency, we would have $\xi = \frac{1}{3}$. Scaling will appear for all time delays larger than the UV cut-off τ_N and smaller than the IR cut-off τ_1. The $x_j(t)$ are independent, positive defined, identical distributed random processes whose time correlation decays with the characteristic time τ_j. The probability distribution of x_j determines the intermittency of the process.

The origin of (A.3) is fairly clear in the context of fully developed turbulence. Indeed we can identify u_n with the velocity difference at scale ℓ_n and x_j with $(\varepsilon_j/\varepsilon_{j-1})^{1/3}$, where ε_j is the energy dissipation at scale ℓ_j.

The following arguments show, that the process defined according to (A.2) and (A.3), is multi-affine: because of the fast decrease of the correlation times $\tau_j = (\ell_j)^\alpha$, the characteristic time of $u_n(t)$ is of the order of the shortest one, i.e. $\tau_n = (\ell_n)^\alpha$. Therefore, the leading contribution to the structure function $\tilde{S}_q(\tau) = \langle\langle |u(t+\tau) - u(t)|^q \rangle\rangle$ with $\tau \sim \tau_n$ stems from the nth term in (A.2). This can be understood nothing that in the sum $u(t+\tau) - u(t) = \sum_{k=1}^{N} [u_k(t+\tau) - u_k(t)]$ the terms with $k \leq n$ are negligible because $u_k(t+\tau) \simeq u_k(t)$ and the terms with $k \geq n$ are sub-leading. Thus one has

$$\tilde{S}_q(\tau_n) \sim \langle |u_n|^q \rangle \sim \langle |g_n|^q \rangle \langle x^q \rangle^n \sim \tau_n^{(\xi q/\alpha) - (\log_2 \langle x^q \rangle)/\alpha} \tag{A.4}$$

and therefore for the scaling exponents

$$\zeta_q = \frac{\xi q}{\alpha} - \frac{\log_2 \langle x^q \rangle}{\alpha}. \tag{A.5}$$

The limit of an affine function can be obtained when all the x_j are equal to one. A proper proof of these result can be found in [45]. Let us notice at this stage that the previous "temporal" signal for $\alpha = 1 - \xi$ is a good candidate for a velocity measurements in a Lagrangian, co-moving, reference frame (see body of the paper). Indeed, in such a reference frame the temporal decorrelation properties at scale ℓ_n are given by the eddy-turn-over times $\tau_n = (\ell_n)^{1-\xi}$.

On the other hand, in the laboratory reference frame the sweeping dominates the time evolution in a fixed point of the space and we must use as characteristic times of the processes $x_n(t)$ the sweeping times $\tau_n^{(s)} = \ell_n$, i.e. $\alpha = 1$.

Appendix B

We have now all the ingredients to perform a merging of temporal and spatial properties of a turbulent signal in order to define stochastic processes able to reproduce in a realistic way both spatial and temporal fluctuations in a Lagrangian reference frame. We just have to merge in a proper way the two previous algorithms. For example, for a d-dimensional multi-affine field such as, say, one of the three components of a turbulent field in a Lagrangian reference frame we can use the following model:

$$v_{\mathrm{L}}(\mathbf{x}, t) = \sum_{n=1}^{N} \sum_{k=1}^{2^{d(n-1)}} a_{n,k}(t)\, \varphi\left(\frac{\mathbf{x} - \mathbf{x}_{n,k}}{\ell_n}\right), \tag{B.1}$$

where the temporal dependency of $a_{n,k}(t)$ is chosen following the sequential algorithm while its spatial part are given by the dyadic structure of the non-sequential algorithm. In (B.1) we have used the notation $v_{\mathrm{L}}(\mathbf{x}, t)$ in order to stress the typical Lagrangian character of such a field.

We are now also able to guess a good candidate for the same field measured in the laboratory-reference frame, i.e. where the time properties are dominated by the sweeping of small scales by large scales. Indeed, it is enough to physically reproduce the sweeping effects by allowing the centre of the wavelets-like functions used to mimic the eddies-like turbulent structures to move according a swept-dynamics.

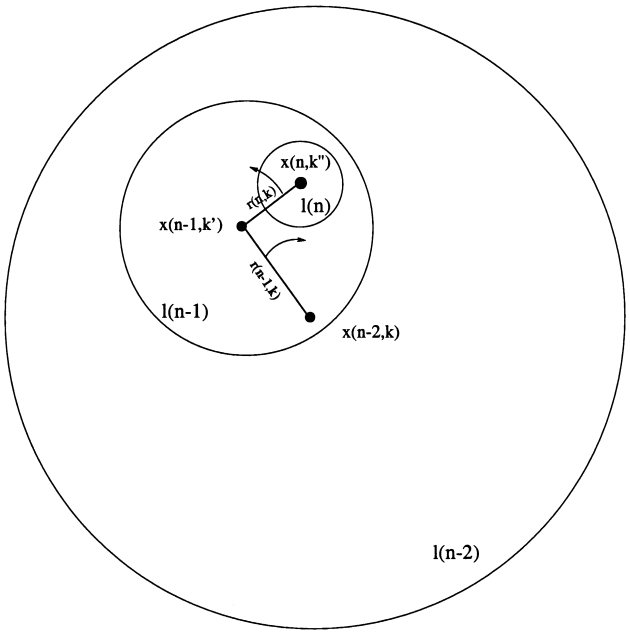

Fig. 11. Sketch of the construction of the synthetic turbulent field. Circles represent symbolically the eddies on the scale n, $n-1$, $n-2$. The centres of the eddies are denoted by x, r indicates the distances between subsequent generations and the arrows hint to the sweeping motion.

To do so, let us define the Eulerian model

$$v_{\mathrm{E}}(\mathbf{x},t)=\sum_{n=1}^{N}\sum_{k=1}^{2^{d(n-1)}}a_{n,k}(t)\,\varphi\left(\frac{\mathbf{x}-\mathbf{x}_{n,k}(t)}{\ell_n}\right), \tag{B.2}$$

where the difference with the previous definition is in the temporal dependency of the centres of the wavelets, $\mathbf{x}_{n,k}(t)$. According to the Richardson–Kolmogorov cascade picture, one assumes that sweeping is present, i.e. $\mathbf{x}_{n,k}=\mathbf{x}_{n-1,k'}+\mathbf{r}_{n,k}$, where (n,k') labels the "mother" of the (n,k)-eddy and $\mathbf{r}_{n,k}$ is a stochastic vector which depends on $\mathbf{r}_{n-1,k'}$ and evolves with characteristic time $\tau_n\propto(\ell_n)^{1-\xi}$. See Fig. 11 for a sketch of the construction. Furthermore, its norm is $\mathrm{O}(\ell_n)$: $c_1<|\mathbf{r}_{n,k}|/\ell_n<c_2$, where c_1 and c_2 are constants of order one.

We now see that if we measure in one fixed spatial point a fluctuations over a time delay δt, is like to measure a simultaneous fluctuations at scale separation $R=U_0\delta t$, i.e. due to the sweeping the main contribution to the sum will be given by the terms with scale-index $n=\log_2(R=U_0\delta t)$ while the temporal dependency of the coefficients $a_{n,k}(t)$ will be practically frozen on that timescale. This happens because in presence of the sweeping the main contribution is given by the displacement of the centre at large scale, i.e. $\delta r_0=|\mathbf{r}_0(t+\delta t)-\mathbf{r}_0(t)|\sim U_0\delta t$, and the eddy-turn-over time at scale ℓ_n is $\mathrm{O}((\ell_n)^{1-\xi})$ always large that the sweeping time $\mathrm{O}(\ell_n)$ at the same scale. In the previous discussion, for sake of simplicity, we did not consider the incompressibility condition. However, one can take into account this constraint by the projection on the solenoidal space.

In conclusion, we have a way to build up a synthetic signal with the proper Eulerian (laboratory) properties, i.e. with sweeping, and also with the proper Lagrangian properties.

References

[1] H. Kantz, T. Schreiber, Nonlinear Time Series Analysis, Cambridge University Press, Cambridge, UK, 1997.
[2] P. Grassberger, Int. J. Theoret. Phys. 25 (1986) 907.
[3] R. Badii, A. Politi, Complexity. Hierarchical Structures and Scaling in Physics, Cambridge University Press, Cambridge, UK, 1997.
[4] C. Shannon, The Bell Syst. Tech. J. 27 (1948) 379.
[5] C. Shannon, The Bell Syst. Tech. J. 27 (1948) 623.
[6] J.P. Eckmann, D. Ruelle, Rev. Mod. Phys. 57 (1985) 617.
[7] P. Grassberger, I. Procaccia, Phys. Rev. A 28 (1983) 2591.
[8] P. Gaspard, X.-J. Wang, Phys. Rep. 235 (1993) 291.
[9] E. Aurell, G. Boffetta, A. Crisanti, G. Paladin, A. Vulpiani, Phys. Rev. Lett. 77 (1996) 1262.
[10] E. Aurell, G. Boffetta, A. Crisanti, G. Paladin, A. Vulpiani, J. Phys. A 30 (1997) 1.
[11] M. Cencini, M. Falcioni, H. Kantz, E. Olbrich, A. Vulpiani, Phys. Rev. E 62 (2000) 427.
[12] A.N. Kolmogorov, Dokl. Akad. Nauk SSSR 119 (1958) 861.
[13] Y. Sinai, Dokl. Akad. Nauk SSSR 124 (1959) 768.
[14] U. Frisch, Turbulence: The Legacy of A.N. Kolmogorov, Cambridge University Press, Cambridge, UK, 1995.
[15] P. Gaspard, X.-J. Wang, Phys. Rev. A 46 (1992) R3000.
[16] A.N. Kolmogorov, IRE Trans. Inf. Theory 1 (1956) 102.
[17] I.M. Gelfand, A.N. Kolmogorov, A.M. Yaglom, (1958) in: A.N. Shiryeyev (Ed.), Selected Works of A.N. Kolmogorov, Vol. III, Kluwer Academic Publishers, Dordrecht, 1993, p. 33.
[18] M. Abel, L. Biferale, M. Cencini, M. Falcioni, D. Vergni, A. Vulpiani, Phys. Rev. Lett. 84 (2000) 6002.
[19] P. Billingsley, Ergodic Theory and Information, Wiley, New York, 1965.
[20] M. Schell, S. Fraser, R. Kapral, Phys. Rev. A 26 (1982) 504.
[21] D. Welsh, Codes and Cryptography, Clarendon Press, Oxford, 1989.
[22] A.I. Khinchin, Mathematical Foundations of Information Theory, Dover Publication, New York, 1957.
[23] A. Neiman, B. Shulgin, V. Anishchenko, W. Ebeling, L. Schimanskygeier, J. Freund, Phys. Rev. Lett. 76 (1996) 4299.
[24] A. Neiman, B. Shulgin, V. Anishchenko, W. Ebeling, L. Schimanskygeier, J. Freund, Phys. Rev. Lett. 77 (1996) 4851.
[25] R. Artuso, E. Aurell, P. Cvitanović, Nonlinearity 3 (1990) 325.
[26] R. Artuso, E. Aurell, P. Cvitanović, Nonlinearity 3 (1990) 361.
[27] T. Schürmann, P. Grassberger, Chaos 6 (1996) 414.

[28] P. Bergé, Y. Pomeau, C. Vidal, Order Within Chaos, Wiley, New York, 1986.
[29] P. Gaspard, X.-J. Wang, Proc. Natl. Acad. Sci. USA 85 (1988) 4591.
[30] X.-J. Wang, Phys. Rev. A 40 (1989) 6647.
[31] G. Paladin, A. Vulpiani, Phys. Rep. 156 (1987) 147.
[32] T. Bohr, M.H. Jensen, G. Paladin, A. Vulpiani, Dynamical Systems Approach to Turbulence, Cambridge University Press, Cambridge, UK, 1998.
[33] L. Biferale, M. Cencini, D. Vergni, A. Vulpiani, Phys. Rev. E 60 (1999) R6295.
[34] M.H. Jensen, Phys. Rev. Lett. 83 (1999) 76.
[35] A. Monin, A. Yaglom, Statistical Fluid Dynamics, Vol. I, MIT Press, Cambridge, MA, 1971.
[36] A. Monin, A. Yaglom, Statistical Fluid Dynamics, Vol. II, MIT Press, Cambridge, MA, 1975.
[37] V.S. L'vov, E. Podivilov, I. Procaccia, Phys. Rev. E 55 (1997) 7030.
[38] G. Boffetta, A. Celani, A. Crisanti, A. Vulpiani, Europhys. Lett. 46 (1999) 177.
[39] G. Boffetta, A. Celani, A. Crisanti, A. Vulpiani, Phys. Rev. E 60 (1999) 6734.
[40] L. Biferale, G. Boffetta, A. Celani, F. Toschi, Physica D 127 (1999) 187.
[41] R. Benzi, L. Biferale, F. Toschi, Phys. Rev. Lett. 80 (1998) 3244.
[42] R. Benzi, L. Biferale, G.R. Chavarria, S. Ciliberto, F. Toschi, Phys. Fluids 11 (1999) 2215.
[43] R. Benzi, L. Biferale, A. Crisanti, G. Paladin, M. Vergassola, A. Vulpiani, Physica D 65 (1993) 352.
[44] A. Juneja, D.P. Lathrop, K.R. Sreenivasan, G. Stolovitzky, Phys. Rev. E 49 (1994) 5179.
[45] L. Biferale, G. Boffetta, A. Celani, A. Crisanti, A. Vulpiani, Phys. Rev. E 57 (1998) R6261.
[46] U. Frisch, M. Vergassola, Europhys. Lett. 14 (1991) 439.
[47] M.H. Jensen, G. Paladin, A. Vulpiani, Phys. Rev. Lett. 67 (1991) 208.
[48] Y. Gagne, B. Castaing, C.R. Acad. Sci. Paris 312 (1991) 441.
[49] B. Mandelbrot, J. Fluid Mech. 72 (1975) 401.
[50] M. Farge, Ann. Rev. Fluid Mech. 24 (1992) 395.
[51] E. Leveque, G. Ruiz-Chavarria, C. Baudet, S. Ciliberto, Phys. Fluids 11 (1999) 1869.
[52] P. Allegrini, J.F. Douglas, S.C. Glotzer, Phys. Rev. E 60 (1999) 5714.